Individual pathways in the formation of magic-size clusters and conventional quantum dots

Zhang, Jing; Hao, Xiaoyu; Rowell, Nelson; Kreouzis, Theo; Han, Shuo; Fan, Hongsong; Zhang, Chunchun; Hu, Changwei; Zhang, Meng; Yu, Kui

Publisher's version / Version de l'éditeur:
https://doi.org/10.1021/acs.jpclett.8b01520
The Journal of Physical Chemistry Letters, 9, 13, pp. 3660-3666, 2018-06-22

THE JOURNAL OF PHYSICAL CHEMISTRY Letters

Letter

Cite This: J. Phys. Chem. Lett. 2018, 9, 3660−3666

pubs.acs.org/JPCL

Individual Pathways in the Formation of Magic-Size Clusters and Conventional Quantum Dots

Jing Zhang,[†] Xiaoyu Hao,[†] Nelson Rowell,[‡] Theo Kreouzis,[§,∥] Shuo Han,[†] Hongsong Fan,[⊥] Chunchun Zhang,[#] Changwei Hu,[∇] Meng Zhang,[*,†] and Kui Yu[*,†,⊥]

[†]Institute of Atomic and Molecular Physics, Sichuan University, Chengdu, Sichuan 610065, People's Republic of China

[‡]National Research Council Canada, Ottawa, Ontario K1A 0R6, Canada

[§]School of Physical Science and Technology, Sichuan University, Chengdu, Sichuan 610065, People's Republic of China

[∥]School of Physics and Astronomy, Queen Mary University of London, London, E1 4NS, United Kingdom

[⊥]Engineering Research Center in Biomaterials, Sichuan University, Chengdu, Sichuan 610065, People's Republic of China

[#]Analytical and Testing Center, Sichuan University, Chengdu, Sichuan 610065, People's Republic of China

[∇]College of Chemistry, Sichuan University, Chengdu, Sichuan 610065, People's Republic of China

Supporting Information

ABSTRACT: The formation relationship between colloidal magic-size clusters (MSCs) and conventional quantum dots (QDs) has not been well established. Here, we report our systematic study on their formation pathways, using cadmium sulfide (CdS) as a model system. Two Cd precursors were prepared from CdO with branched 2-methyloctadecanoic acid ($C_{16}H_{33}CH(CH_3)-COOH$) and linear oleic acid ($C_{16}H_{31}CH_2-COOH$), reacting with elemental S powder in 1-octadecene (ODE). We show that the presence of MSC-311 (exhibiting a sharp absorption peaking at 311 nm) is regulated by the growth of conventional QDs. We demonstrate that MSC-311 cannot directly convert into conventional QDs but to its immediate precursor (IP-311), which is transparent in optical absorption (>310 nm). We propose that there are two individual pathways for the formation of MSCs and conventional QDs, linked by an intrinsic pathway from MSCs to IPs to fragments to QDs. The present study introduces new avenues to precisely control their formation.

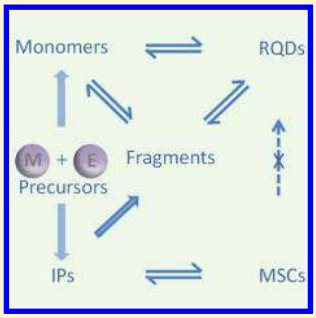

The growth relationship between colloidal magic-size clusters (MSCs) and conventional quantum dots (QDs) has been addressed only in a limited fashion, with no consensus reached in the literature.[1−8] Compared with conventional QDs, also called regular QDs (RQDs), MSCs exhibit narrower optical bandwidths due to much tighter size distributions.[9−20] At the same time, the absorption feature of RQD samples extracted from a reaction batch can continuously red-shift due to the growth in size, while that of MSC samples persistently occurs at fixed wavelengths.[21−24]

While MSCs are generally produced together with RQDs,[4−8] single-ensemble MSCs (such as CdTe MSC-371, CdS MSC-311, CdS MSC-322, and CdSe MSC-415 exhibiting absorption peaking respectively at 371, 311, 322, and 415 nm) without the coproduction of RQDs have been achieved recently via our two-step approach.[1,2,17,18] The first step is the preparation of the immediate precursors (IPs) of MSCs, performed at a relatively high temperature but limited to the induction period prior to nucleation and growth of RQDs. The second-step is the IP to MSC transformation, carried out at a relatively low temperature. The synthesis of single-ensemble MSCs without the complication of other-size nanocrystals (NCs) via the two-step approach has added critical information on the induction period, together with structural transformations from CdS IPs to CdS MSC-311 and between CdS MSC-311 and CdS MSC-322, which occurs with first-order reaction kinetics.[2,18] The growth relationship between MSCs and RQDs remains, however, poorly understood, together with the fate of MSCs in reactions.

Herein, we report a systematic study on the formation pathways of RQDs and MSCs, using CdS as a model system via our two-step approach. The CdS RQDs and/or MSC-311 were synthesized via a heating up approach in noncoordinating solvent 1-octadecene (ODE). Phosphorus-containing compounds, such as tri-*n*-octylphosphine or diphenylphosphine, were avoided by applying elemental sulfur (S) directly. Both linear oleic acid ($C_{16}H_{31}CH_2COOH$, denoted Acid A) and branched 2-methyloctadecanoic acid ($C_{16}H_{33}CH(CH_3)-COOH$, denoted Acid B) were used to respectively prepare two Cd precursors, CdA_2 and CdB_2, from cadmium oxide (CdO) in ODE. We show that the growth of conventional QDs is accompanied by the synchronized disappearance of IPs (Figures 1 and 2) and of MSCs (Figure 3), and MSCs cannot directly convert to RQDs, but to their immediate precursors (IPs) (Figure 3). We demonstrate that the formation pathway

Received: May 14, 2018
Accepted: June 11, 2018
Published: June 22, 2018

DOI: 10.1021/acs.jpclett.8b01520
J. Phys. Chem. Lett. 2018, 9, 3660−3666

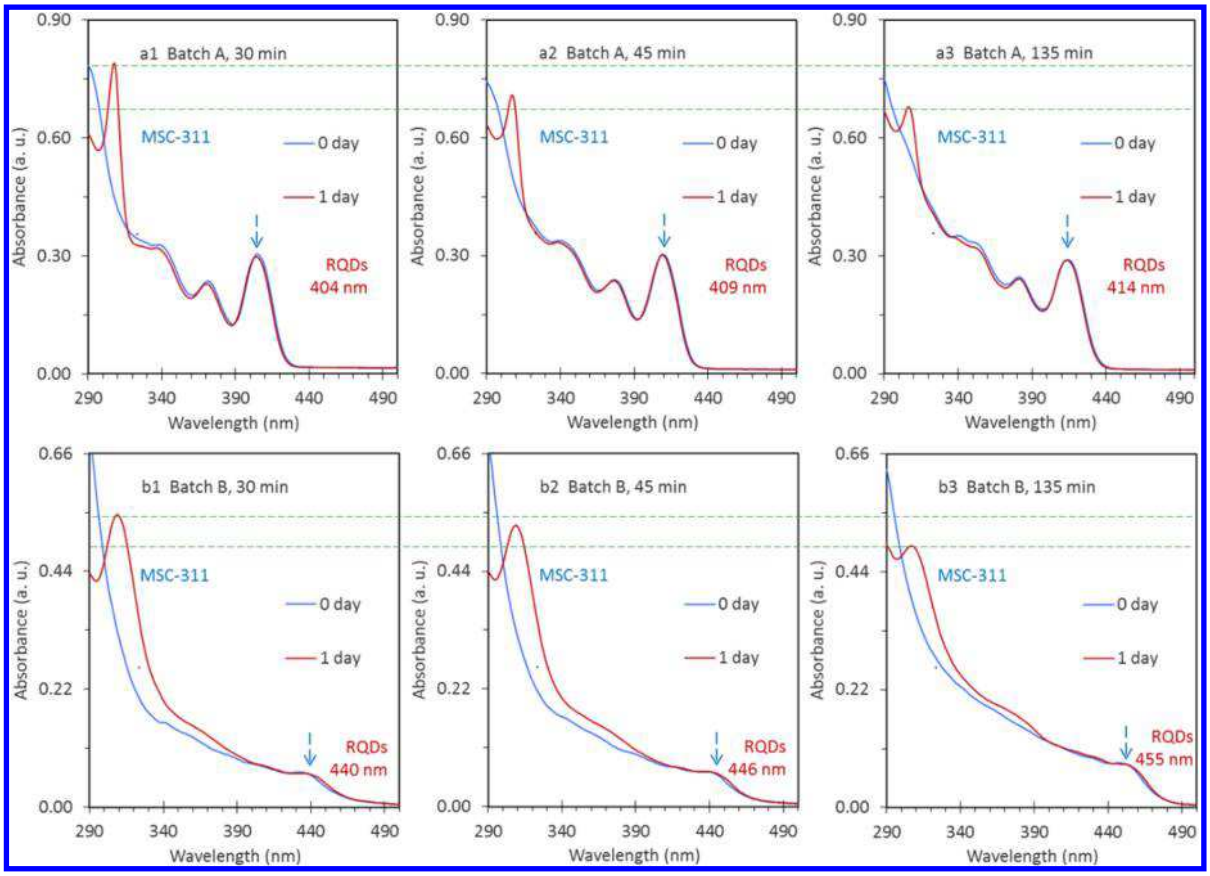

Figure 1. Optical absorption spectra of samples extracted from Batch A (top) and B (bottom) in ODE at 230 °C for (1) 30, (2) 45, and (3) 135 min. Absorption measurements were carried out immediately (blue traces, 0 day) and after one-day storage (red traces, 1 day). The dashed lines are visual guides; evidently, MSC-311 formed after storage, and its absorbance decreased along with the growth of RQDs.

of MSCs and RQDs can be finely tuned via the addition of Acid B to CdA_2 and S reactions (Figure 4). For our experimental observation of the relatively high reactivity of CdA_2 compared to that of CdB_2 and the relative high coordination of Acid B to Cd, we try to understand with the acidity effect of Acids A and B, using density functional theory (DFT) calculations and nuclear magnetic resonance (NMR) (Figure 5). On the basis of the experimental data, we propose a model, detailed in Scheme 1, which comprises two pathways from reaction precursors via monomers and fragments to RQDs (top), as well as via IPs to MSCs (bottom). Scheme 1 suggests the existence of the intrinsic pathway from MSCs to IPs to fragments to RQDs. The present study contributes to narrowing the knowledge gap on the relationship of formation pathways of MSCs and RQDs.

Figure 1 shows the optical absorption spectra collected from samples taken from Batches A (top panel) and B (bottom panel) at 230 °C. The samples (25 μL each) were dispersed in a mixture of toluene (2.95 mL) and methanol (0.05 mL). Our previous study on the CdS IP to CdS MSC-311 structural transformation suggested that the transformation proceeded relatively fast in toluene than in cyclohexane, and was accelerated by the presence of a trace amount of methanol.[2] Also, the presence of a trace amount of methanol speeded up the CdS MSC-322 to CdS MSC-311 structural transformation.[18] In the present study, we used thus the toluene and methanol mixture. The spectra were collected immediately (blue traces, 0 day) and after one-day storage (red traces, 1 day). The absorption spectra of the 30, 45, and 135 min samples are shown in parts 1, 2, and 3 of Figure 1, respectively. During the reaction period of 15 to 135 min, six samples were extracted from each of the two batches, and their absorption spectra are presented by Figures S1-1 (Batch A) and S1-2 (Batch B).

The immediately collected spectra (blue traces, 0 day) display broad absorption peaks corresponding to the presence of RQDs. The redshift of the peaks (from 404 to 414 nm (top) and from 440 to 455 nm (bottom)) indicates the growth of the RQDs during the reaction period from 30 to 135 min. Over the growth period, the size of the RQDs in Batch A is much smaller than in Batch B and with significantly more particles, suggesting that the reactivity of CdA_2 is higher than that of CdB_2. Regarding the reactivity difference, Figure S1-3 presents additional comparisons for the Batch A and B samples. None of the reaction products displayed sharp absorption peaking at 311 nm on day 0.

After one-day storage (red traces, 1 day), the RQDs changed little in both size and population. Interestingly, one additional absorption peaking at ~311 nm was detected in each of the samples, together with a noticeable decrease of the absorbance at 290 nm (presumably due to the IP → MSC transformation).[2] The sharp peak is attributed to the presence of MSC-311 via intramolecular reorganization (as shown by the IP → MSC pathway in Scheme 1).[1,2,17,18] The IPs generated at 230 °C are transparent in optical absorption (at wavelengths >310 nm), but contribute to the overall absorption at shorter wavelengths as do the monomers and fragments. The IP → MSC conversion is consistent with the absorption decrease at

DOI: 10.1021/acs.jpclett.8b01520
J. Phys. Chem. Lett. 2018, 9, 3660−3666

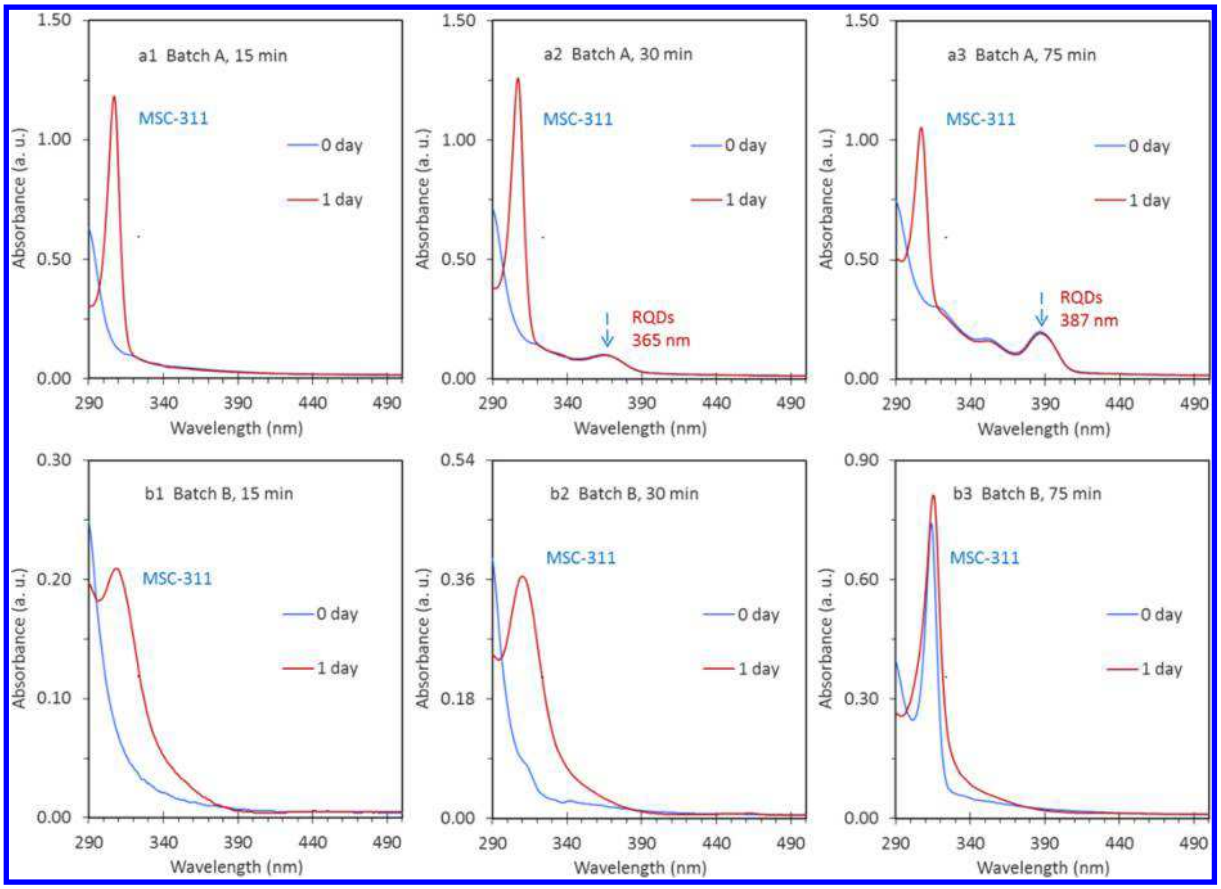

Figure 2. Optical absorption spectra of samples extracted from Batch A (a) and B (b) at 180 °C for (1) 15, (2) 30, and (3) 75 min. Absorption measurements were carried out immediately (blue traces, 0 day) and after one-day storage (red traces, 1 day). Note that MSC-311 was detected in the latter reaction stage of Batch B (b3, blue trace).

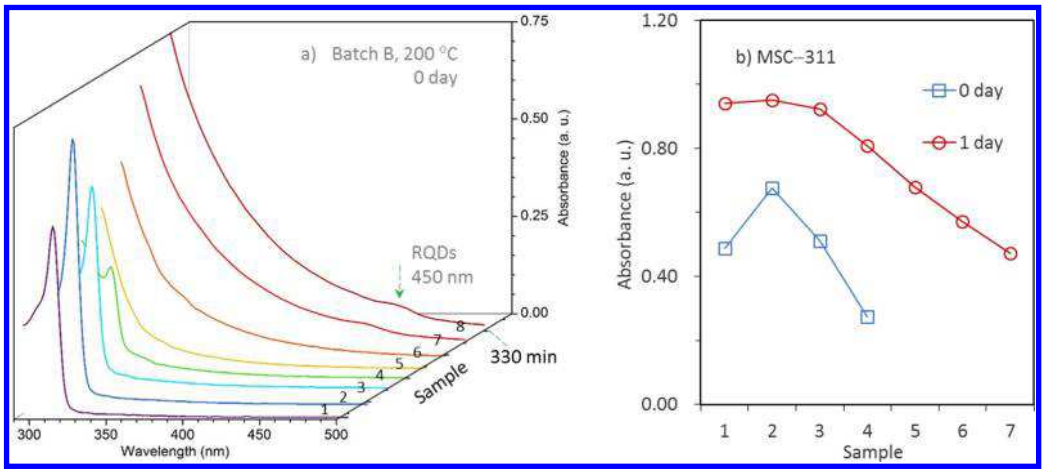

Figure 3. (a) Optical Absorption spectra of samples extracted from Batch B at 200 °C for (1) 15, (2) 60, (3) 120, (4) 180, (5) 210, (6) 270, (7) 300 and (8) 330 min (b) Comparison of the absorbance of MSC-311 monitored from the Batch B sample dispersions before (blue squares, 0 day) and after the one-day storage (red circles, 1 day). For Samples 4 to 6, we note the complete disappearance of MSC−311 without any noticeable growth of RQDs on day 0, together with reappearance of MSC-311 on day 1.

290 nm from day 0 to day 1. It is noteworthy that the formation of MSCs during one-day storage was, for sure, not resulted from the interaction between the Cd and S precursors; the formation of Cd−S bonds for Batch A requires a temperature higher than 120 °C.[2]

Both batches displayed a decrease in the optical density of MSC-311 over time. Evidently, the growth of the RQDs appears linked by the decrease of MSC-311. The former requires the addition of monomers and/or fragments, while the latter is indicative of a decrease in IP population as the reaction progressed. Thus, the experimental observation, RQD growth accompanied by MSC reduction, is in agreement with the IP to fragment to RQD pathway shown in Scheme 1.

Figure 2 presents the absorption spectra of three samples extracted from Batch A (top panel) and Batch B (bottom panel) at 180 °C after 15 (a1 and b1), 30 (a2 and b2), and 75

DOI: 10.1021/acs.jpclett.8b01520
J. Phys. Chem. Lett. 2018, 9, 3660−3666

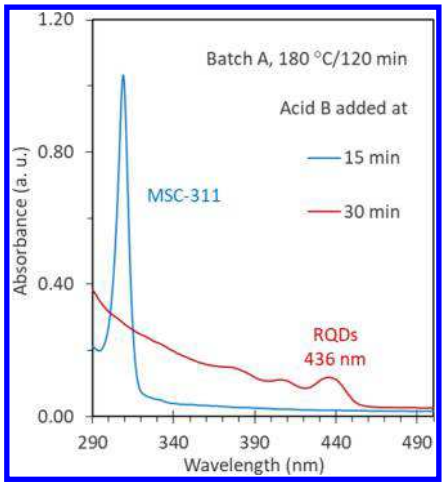

Figure 4. Optical absorption spectra of two samples extracted from Batch A at 180 °C with the growth period of 120 min; the addition of Acid B was performed at 15 (blue trace) and 30 (red trace) min. The separate production of MSCs and RQDs supports the existence of two formation pathways.

Scheme 1. Schematic Drawing of the Separate Pathways Proposed for the Formation of RQDs (Top) and MSCs (Bottom)[a]

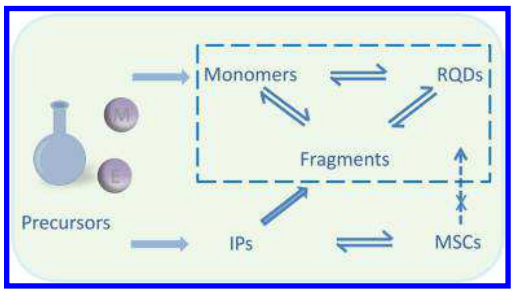

[a]The formation of RQDs follows the conventional view to start with monomers and/or fragments.[25−28] The development of MSCs is via the structural transformation from their immediate precursors (IPs).[1,2] MSCs are not nuclei of RQDs, and their direct evolution to RQDs is disallowed. The growth of RQDs accompanied by the decrease of MSCs is via the dissolution pathway back to IPs, and further decomposition of the IP to fragments.

min (a3 and b3). The two batches were identical to those of Figure 1, except for the lower reaction temperature, which should have resulted in longer induction periods prior to nucleation and growth of RQDs. Samples were dispersed and measured in the same way as what was done for Figure 1. Six samples were extracted from each of the two batches during the reaction period from 5 to 75 min, and their absorption spectra are presented in Figures S2-1 for Batch A and S2-2 for Batch B.

For Batch A (Figures 2, top, and S2-1, blue traces, 0 day), RQDs became apparent at 30 min, exhibiting a broad absorption peaking at 365 nm and red-shifting at longer reaction periods. Thus, the induction period lasted at least 15 min (Figure S2-1), prior to nucleation and growth of RQDs. After the one-day storage (red traces, 1 day), MSC-311 evolved from each of the six samples, and the absorption at 290 nm decreased. Again, in the absence of RQDs, the amount of MSC-311 increased up to 20 min, indicating the proliferation and longevity of the IP in the reaction. Coinciding with the growth of RQDs during the 30 to 75 min period, the population of MSC-311 decreased, suggesting that the competition between the production processes of MSCs and RQDs occurs generally, as also observed for Batches A and B (Figure 1).

For Batch B (Figures 2, bottom, and S2−2, blue traces, 0 day), there was no nucleation and growth of RQDs over a reaction period of 75 min. At the same time, the 5, 15, and 20 min samples were essentially transparent in optical absorption (at wavelengths longer than 310 nm). MSCs started to be present at 30 min, and increased in population up to 75 min, exhibiting narrow absorption peaking at ∼311 nm for the 45 and 70 min samples. After one-day storage (red traces, 1 day), MSC-311 was not detected for the 5 min sample, but was for all the other samples together with an absorption decrease at 290 nm. For the 45 and 70 min samples, a small increase for MSC-311 was observed.

Comparing Batches A and B samples (blue traces), we notice that the absorption at 290 nm of Batch A samples is higher than that of the corresponding Batch B samples. This is consistent with the presumption that the reactivity of CdA_2 is higher than that of CdB_2. For the 45 and 75 min samples, MSC-311 evidently formed in Batch B but not in Batch A,

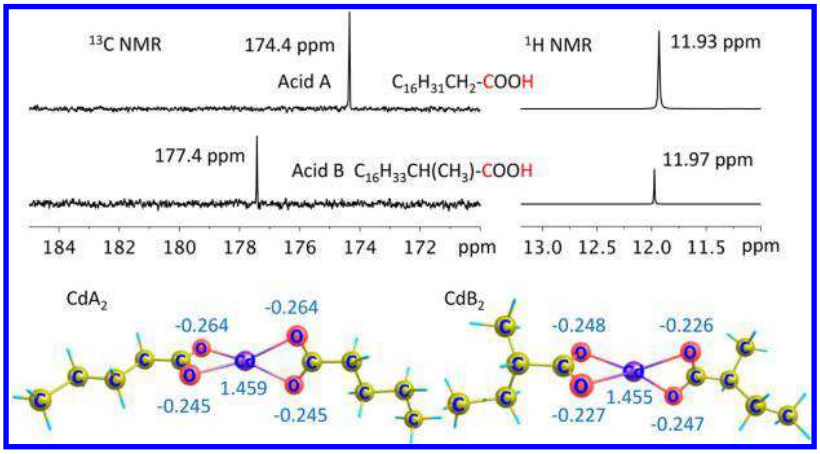

Figure 5. (Top) ^{13}C NMR (left) and ^{1}H NMR (right) of Acids A and B. The relatively downfield signals of Acid B suggests its relatively strong acidity. (Bottom) DFT calculations of the two molecules for CdA_2 (left) and CdB_2 (right). The partial charge (a.u.) of one Cd atom and four O atoms are indicated, with the sum of the absolute values of 2.477 and 2.403, respectively, suggesting that the former is more reactive than the latter.

DOI: 10.1021/acs.jpclett.8b01520
J. Phys. Chem. Lett. 2018, 9, 3660−3666

suggesting an improved thermostability of MSC-311 with CdB_2.

For Batch B (blue traces, 0 day), the production of MSCs without RQDs at 180 °C (Figure 2, bottom) and of RQDs without MSCs at 230 °C (Figure 1, bottom) further reflects the competitive relationship between the MSC and RQD production processes. As shown in Scheme 1, a relatively low reactivity condition (such as 180 °C) allow the IP to form MSCs without decomposing into fragments. By contrast, a relatively high reactivity condition (such as 230 °C) leads to the depletion of the IP to fragments, which feeds the growth of RQDs. To further elaborate the two growth pathways for RQD and MSC formation, we studied Batch B at 200 °C, expecting an evolution of MSCs without RQDs initially, followed by the disappearance of MSCs and the growth of RQDs.

Figure 3a presents the temporal evolution of absorption of samples extracted from Batch B at 200 °C. The same dispersion preparation and measurements were carried out, as used for Figures 1 and 2. As shown by Figure 3a, the population MSC-311 increased up to 60 min, and then decreased. At 180 min, there was a small amount of MSC-311 left; meanwhile, nucleation and growth of RQDs seemed to have taken place. For the 210 and 270 min samples, MSC-311 completely disappeared, and the RQDs did not grow much. For the 300 to 330 min samples, RQDs were observed eventually with bandgap absorption peaking at ∼435 and ∼445 nm, respectively. The complete disappearance of MSC-311 without a noticeable growth of RQDs (during the growth period of 180 to 270 min) provides strong experimental evidence that MSCs are not the nuclei of RQDs, as depicted in the forbidden path on the right-hand side of Scheme 1. For the eight sample dispersions, absorption spectra were collected on the second day. Figure S3 shows the optical absorption spectra of the samples with blue and red traces for day 0 and 1, respectively.

Figure 3b displays the optical density of MSC-311 detected from the first seven samples extracted from Batch B at 200 °C, with blue squares (day 0) and red circles (day 1). The magnitude of the MSC-311 optical density on day 1 is indicative of the amount of the IP produced at 200 °C (on day 0). Interestingly, the amount of the IP generated at 200 °C at the beginning (15 min, Sample 1) seemed to change little up to 120 min (Sample 3), as indicated by the MSC-311 optical density obtained on day 1. Furthermore, the amount of the IP at 200 °C started to decrease at 180 min (Sample 4), while disappearing almost completely at 330 min (Sample 8). Again, the nucleation and growth of RQDs (at 180 min) resulted in fragmentation of the IP, thus the decreased presence (up to 300 min (Sample 7)) or absence (at 330 min) of MSC-311 after the one-day storage. The presence of MSC-311 in significant amounts in the 210 and 270 min samples (Samples 5 and 6) on day 1 can well be attributed to the MSC to IP pathway shown in Scheme 1. At 200 °C, importantly, MSC-311 fully dissolved back to the IP (for Samples 5 and 6).

Naturally, the different influences of CdA_2 and CdB_2 on the formation of RQDs and MSCs drew our attention to use mixtures of Acids A and B to prepare the Cd precursor. A detailed study can be found in Figure S4-1, which shows the absorption of samples from four different batches at 200 °C, in which four mixtures of the two acids were used. Again, the growth of RQDs inhibited that of MSC-311. For the mixture with the equal molar ratio of Acid A and B, the resulting product was mainly MSC-311, suggesting that the formation of CdB_2 occurs more readily than that of CdA_2 due to the stronger coordination of Acid B than Acid A to Cd. This is in agreement with the observed lower reactivity of CdB_2 than that of CdA_2. We therefore investigated the use of Acid B as an additive to Batch A, with the addition performed before (at 15 min) and after (at 30 min) the nucleation and growth of RQDs at 180 °C.

Figure 4 illustrates the effect of the addition of Acid B (1.75 mmol) to Batch A (with 1.32 mmol Acid A used) at 180 °C. Interestingly, MSCs and RQDs were obtained, respectively, when Acid B was added to Batch A before (at 15 min, blue trace) and after (at 30 min, red trace) nucleation and growth of RQDs. This is further detailed in Figure S4-2, where temporal evolution of absorption of samples extracted from the two Batch A is shown. For the former batch, MSC-311 steadily increased. For the latter batch, the RQDs kept growing, while the initial presence of MSC-311 was followed by rapid decrease and disappearance. Evidently, the disappearance of MSC-311 is related to the growth of RQDs. The experiments were repeated with the same (1.75 mmol) and less (0.35 mmol) amounts of Acid B, as shown in the left and right parts of Figure S4-3, respectively. When tuning the growth pathway of MSCs vs RQDs in Batch A at 180 °C, the amount of acid B added is critical.

Based on the experimental results, we proposed the two pathways for the formation of RQDs and MSCs, as illustrated by Scheme 1. Let us briefly review the experimental results related to Acid B. Batch B at 230 °C (Figure 1) produced RQDs and no MSC-311 (on day 0), together with monomers, fragments, and IPs. The IP-to-MSC conversion was detected after one-day storage at a lower temperature. The IP to fragment to RQD pathway is supported by the size increase of the RQDs (on day 0), coinciding with a population decrease of MSC-311 (on day 1 monitored); the decrease could be resulted from decreased IP-311 (produced on day 0). Batch B at 180 °C (Figure 2) produced MSC-311 (on day 0) but no RQDs. Accordingly, the relatively high and low temperatures favor the formation of RQDs and MSCs, respectively, via their individual formation pathways. Batch B at 200 °C (Figure 3) produced MSC-311 (on day 0) at an initial stage but RQDs only at a later stage. Thus, the two pathways for the formation of RQDs and MSCs should be interlinked, as proposed in Scheme 1 via the MSC to IP to fragment to RQD pathway. Moreover, it is practical to control the formation of MSCs in Batch A at 180 °C via the addition of Acid B (Figure 4). Scheme 1 includes, as indicated by the dashed squared area, the conventional concept about the nucleation and growth RQDs, which takes place from monomers and/or fragments (including dimers and trimers), with the fragments resulted from monomers.[25−28] Scheme 1 illustrates further the existence of another pathway, the formation of the IP which transforms to MSCs, with the direct conversion of MSCs into RQDs not allowed. Moreover, the growth of RQDs accompanied by a decrease in MSCs occurs via the MSC to IP to fragment to RQD pathway.

The present study is based on the use of Acids A and B, with two corresponding Cd precursors, CdA_2 and CdB_2 (Figures 1−3), and the addition of Acid B to Batch A (Figure 4). CdA_2 is more reactive than CdB_2 (Figures 1 and 2), and Acid B coordinates more readily to Cd than Acid A (Figure 4). These experimental observations are in agreement with the relatively high acidity of Acid B compared to Acid A. NMR and DFT have been used to study the chemistry involved in the

DOI: 10.1021/acs.jpclett.8b01520
J. Phys. Chem. Lett. 2018, 9, 3660−3666

formation of monomers, fragments, and RQDs and MSCs.[29−32] Figure 5 shows NMR study (top) of Acids A and B and DFT calculations of two molecules for CdA_2 and CdB_2. Figures S5-1a and S5-1b present the ^{13}C NMR and ^{1}H NMR measurements with assignments for C and H resonance signals, respectively. For Acids A and B, the carbon resonance signals of the carbonyl groups (C═O) are at 174.4 and 177.4 ppm in the ^{13}C NMR spectra (top left), respectively, with the proton resonance signals of the carboxyl group (C = (O)O−H) in the ^{1}H NMR spectra at 11.93 and 11.97 ppm (top right). The two relatively downfield signals of Acid B suggest that the acidity of Acid B is relatively high. Additional DFT information is presented in Figure S5-2 for the two Cd precursors, CdA_2 and CdB_2. Figure S5-3 shows X-ray photoelectron spectroscopy (XPS) of CdA_2 and CdB_2. Accordingly, we argue that the relatively high acidity of Acid B results in the relatively low reactivity of CdB_2 and the relatively strong coordination to Cd.

In conclusion, we systematically studied the formation of RQDs and MSCs, using CdS as a model system. We employed two carboxylate acids: linear oleic acid ($C_{16}H_{31}CH_2$−COOH, Acid A) and branched 2-methyloctadecanoic acid ($C_{16}H_{33}CH$-(CH_3)-COOH, Acid B). We found out that CdA_2 has a higher reactivity than CdB_2 toward S, and Acid B has a higher coordination capability than Acid A toward Cd. For Batch B with CdB_2, in particular, we show that high (230 °C) and low (180 °C) reactivity conditions favors the formation of RQDs and MSCs, respectively. Moreover, we have identified an intermediate reaction temperature 200 °C, at which it is possible to demonstrate the growth of RQDs accompanied by the decrease of MSCs, with the presence of MSCs in the initial stage and RQDs at the later stage. Furthermore, we elucidate that MSCs could be obtained from Batch A with CdA_2 at 180 °C, when Acid B was added in the induction period, while RQDs were obtained without addition or when the addition was performed after the induction period. Thus, we propose that RQDs and MSCs have their own individual pathways for their formation. For the growth of RQDs accompanied by the disappearance of MSCs, we attribute to the MSC to IP to fragment to RQD pathway. MSCs would not appear to be the nuclei of RQDs; instead, they dissolve back to IPs (which transformed to MSCs on the second day). Based on our two-step approach to single-ensemble CdTe,[1] CdS,[2,18] and CdSe MSCs[17] without the coexistence of RQDs, we proposed a so-called Yu Pathway to describe the general formation of semiconductor MSCs and RQDs. Also, a process of proton-mediated ligand exchange repeated itself leading to the formation of monomers, IPs, MSCs, and RQDs.[1,2,17,18,29−32] We argued the monomer to be M_2E_n, with M = Cu (I), Zn (II), Cd (II), Pb (II), Ge (II), and In (III), and E = S, Se, and Te.[32] For the Yu model, the IPs and their corresponding MSCs have similar numbers of Cd atoms and E atoms, as demonstrated by CdS IPs and CdS MSC-311.[2] The present work brings deeper insight into the formation of MSCs and RQDs with their individual pathways and introduces the practical control of their formation.

■ ASSOCIATED CONTENT

Supporting Information

The Supporting Information is available free of charge on the ACS Publications website at DOI: 10.1021/acs.jpclett.8b01520.

Experimental details including synthesis and characterization, with absorption spectra, NMR, DFT, and XPS (PDF)

■ AUTHOR INFORMATION

Corresponding Authors

*E-mail: mengzhang@scu.edu.cn.
*E-mail: kuiyu@scu.edu.cn.

ORCID

Shuo Han: 0000-0003-0880-1833
Hongsong Fan: 0000-0003-3812-9208
Kui Yu: 0000-0003-0349-2680

Notes

The authors declare no competing financial interest.

■ ACKNOWLEDGMENTS

K.Y. thanks the National Natural Science Foundation of China (NSFC) 21573155 and 21773162 and the Fundamental Research Funds for the Central Universities SCU2015A002. We thank Open Project of Key State Laboratory for Supramolecular Structures and Materials of Jilin University for SKLSSM 201830. We thank Dr. Ke Wang, Prof. Mingli Yang, Miss Ting Qi, Prof. Huaqing Yang, Prof. Jianyi Ma, and Prof. Fan Wang for useful guidance and discussions for our DFT calculations. We thank Miss Tingting Zhu for her help on storage stability studied and Mr. Junbing Tang for a valuable discussion on partial charge.

■ REFERENCES

(1) Liu, M.; Wang, K.; Wang, L.; Han, S.; Fan, H.; Rowell, N.; Ripmeester, J. A.; Renoud, R.; Bian, F.; Zeng, J.; Yu, K. Probing Intermediates of the Induction Period Prior to Nucleation and Growth of Semiconductor Quantum Dots. *Nat. Commun.* **2017**, *8*, 15467.

(2) Zhu, T.; Zhang, B.; Zhang, J.; Lu, J.; Fan, H.; Rowell, N.; Ripmeester, J. A.; Han, S.; Yu, K. Two-Step Nucleation of CdS Magic-Size Nanocluster MSC-311. *Chem. Mater.* **2017**, *29*, 5727−5735.

(3) Friedfeld, M. R.; Stein, J. L.; Cossairt, B. M. Main-Group-Semiconductor Cluster Molecules as Synthetic Intermediates to Nanostructures. *Inorg. Chem.* **2017**, *56*, 8689−8697.

(4) Gary, D. C.; Terban, M. W.; Billinge, S. J. L.; Cossairt, B. M. Two-Step Nucleation and Growth of InP Quantum Dots via Magic-Sized Cluster Intermediates. *Chem. Mater.* **2015**, *27*, 1432−1441.

(5) Jiang, Z. J.; Kelley, D. F. Role of Magic-Sized Clusters in the Synthesis of CdSe Nanorods. *ACS Nano* **2010**, *4*, 1561−1572.

(6) Yu, K.; Hu, M. Z.; Wang, R.; Piolet, M. L.; Frotey, M.; Zaman, M. B.; Wu, X.; Leek, D. M.; Tao, Y.; Wilkinson, D.; Li, C. Thermodynamic Equilibrium-Driven Formation of Single-Sized Nanocrystals: Reaction Media Tuning CdSe Magic-Sized versus Regular Quantum Dots. *J. Phys. Chem. C* **2010**, *114*, 3329−3339.

(7) Pan, D.; Ji, X.; An, L.; Lu, Y. Observation of Nucleation and Growth of CdS Nanocrystals in a Two-Phase System. *Chem. Mater.* **2008**, *20*, 3560−3566.

(8) Peng, Z. A.; Peng, X. Nearly Monodisperse and Shape-Controlled CdSe Nanocrystals via Alternative Routes: Nucleation and Growth. *J. Am. Chem. Soc.* **2002**, *124*, 3343−3353.

(9) Kasuya, A.; Sivamohan, R.; Barnakov, Y. A.; Dmitruk, I. M.; Nirasawa, T.; Romanyuk, V. R.; Kumar, V.; Mamykin, S. V.; Tohji, K.; Jeyadevan, B.; Shinoda, K.; Kudo, T.; Terasaki, O.; Liu, Z.; Belosludov, R. V.; Sundararajan, V.; Kawazoe, Y. Ultra-Stable Nanoparticles of CdSe Revealed from Mass Spectrometry. *Nat. Mater.* **2004**, *3*, 99−102.

(10) Yu, Q.; Liu, C. Y. Study of Magic-Size-Cluster Mediated Formation of CdS Nanocrystals: Properties of the Magic-Size Clusters

DOI: 10.1021/acs.jpclett.8b01520
J. Phys. Chem. Lett. 2018, 9, 3660−3666

and Mechanism Implication. *J. Phys. Chem. C* **2009**, *113*, 12766−12771.
(11) Dukes, A. D.; McBride, J. R.; Rosenthal, S. J. Synthesis of Magic-Sized CdSe and CdTe Nanocrystals with Diisooctylphosphinic Acid. *Chem. Mater.* **2010**, *22*, 6402−6408.
(12) Zanella, M.; Abbasi, A. Z.; Schaper, A. K.; Parak, W. J. Discontinuous Growth of II-VI Semiconductor Nanocrystals from Different Materials. *J. Phys. Chem. C* **2010**, *114*, 6205−6215.
(13) Cossairt, B. M.; Owen, J. S. CdSe clusters: At the Interface of Small Molecules and Quantum Dots. *Chem. Mater.* **2011**, *23*, 3114−3119.
(14) Cossairt, B. M.; Juhas, P.; Billinge, S.; Owen, J. S. Tuning the Surface Structure and Optical Properties of CdSe Clusters Using Coordination Chemistry. *J. Phys. Chem. Lett.* **2011**, *2*, 3075−3080.
(15) Kurihara, T.; Noda, Y.; Takegoshi, K. Quantitative Solid-State NMR Study on Ligand−Surface Interaction in Cysteine-Capped CdSe Magic-Sized Clusters. *J. Phys. Chem. Lett.* **2017**, *8*, 2555−2559.
(16) Nevers, D. R.; Williamson, C. B.; Savitzky, B. H.; Hadar, I.; Banin, U.; Kourkoutis, L. F.; Hanrath, T.; Robinson, R. D. Mesophase Formation Stabilizes High-Purity Magic-Sized Clusters. *J. Am. Chem. Soc.* **2018**, *140*, 3652−3662.
(17) Zhu, D.; Hui, J.; Rowell, N.; Liu, Y.; Chen, Q. Y.; Steegemans, T.; Fan, H.; Zhang, M.; Yu, K. Interpreting the Ultraviolet Absorption in Spectrum of 415-nm-Bandgap CdSe Magic-Size Clusters. *J. Phys. Chem. Lett.* **2018**, *9*, 2818−2824.
(18) Zhang, B.; Zhu, T.; Ou, M.; Rowell, N.; Fan, H.; Han, J.; Tan, L.; Dove, M. T.; Ren, Y.; Zuo, X.; Han, S.; Zeng, J.; Yu, K. Thermally-Induced Reversible Structural Isomerization in Colloidal Semiconductor CdS Magic-Size Clusters. *Nat. Commun.* **2018**, DOI: 10.1038/s41467-018-04842-0.
(19) Empedocles, S. A.; Neuhauser, R.; Shimizu, K.; Bawendi, M. G. Photoluminescence from Single Semiconductor Nanostructures. *Adv. Mater.* **1999**, *11*, 1243−1256.
(20) Cui, J.; Beyler, A. P.; Marshall, L. F.; Chen, O.; Harris, D. K.; Wanger, D. D.; Brokmann, X.; Bawendi, M. G. Direct Probe of Spectral Inhomogeneity Reveals Synthetic Tunability of Single-Nanocrystal Spectral Linewidths. *Nat. Chem.* **2013**, *5*, 602−606.
(21) Kudera, S.; Zanella, M.; Giannini, C.; Rizzo, A.; Li, Y.; Gigli, G.; Cingolani, R.; Ciccarella, G.; Spahl, W.; Parak, W. J.; Manna, L. Sequential Growth of Magic-Size CdSe Nanocrystals. *Adv. Mater.* **2007**, *19*, 548−552.
(22) Dagtepe, P.; Chikan, V.; Jasinski, J.; Leppert, V. J. Quantized Growth of CdTe Quantum Dots; Observation of Magic-Sized CdTe Quantum Dots. *J. Phys. Chem. C* **2007**, *111*, 14977−14983.
(23) Ouyang, J.; Kuijper, J.; Brot, S.; Kingston, D.; Wu, X.; Leek, D. M.; Hu, M. Z.; Ripmeester, J. A.; Yu, K. Photoluminescent Colloidal CdS Nanocrystals with High Quality via Noninjection One-Pot Synthesis in 1-Octadecene. *J. Phys. Chem. C* **2009**, *113*, 7579−7593.
(24) Yu, K.; Ouyang, J.; Leek, D. M. In-Situ Observation of Nucleation and Growth of PbSe Magic-Sized Nanoclusters and Regular Nanocrystals. *Small* **2011**, *7*, 2250−2262.
(25) Rempel, J. Y.; Bawendi, M. G.; Jensen, K. F. Insights into the Kinetics of Semiconductor Nanocrystal Nucleation and Growth. *J. Am. Chem. Soc.* **2009**, *131*, 4479−4489.
(26) Xie, L.; Shen, Y.; Franke, D.; Sebastian, V.; Bawendi, M. G.; Jensen, K. F. Characterization of Indium Phosphide Quantum Dot Growth Intermediates Using MALDI-TOF Mass Spectrometry. *J. Am. Chem. Soc.* **2016**, *138*, 13469−13472.
(27) García-Rodríguez, R.; Hendricks, M. P.; Cossairt, B. M.; Liu, H.; Owen, J. S. Conversion Reactions of Cadmium Chalcogenide Nanocrystal Precursors. *Chem. Mater.* **2013**, *25*, 1233−1249.
(28) Sowers, K. L.; Swartz, B.; Krauss, T. D. Chemical Mechanisms of Semiconductor Nanocrystal Synthesis. *Chem. Mater.* **2013**, *25*, 1351−1362.
(29) Yu, K.; Liu, X.; Zeng, Q.; Leek, D. M.; Ouyang, J.; Whitmore, K. M.; Ripmeester, J. A.; Tao, Y.; Yang, M. Effect of Tertiary and Secondary Phosphines on Low-Temperature Formation of Quantum Dots. *Angew. Chem., Int. Ed.* **2013**, *52*, 4823−4828.
(30) Yu, K.; Liu, X.; Zeng, Q.; Yang, M.; Ouyang, J.; Wang, X.; Tao, Y. The Formation Mechanism of Binary Semiconductor Nanomaterials: Shared by Single-Source and Dual-Source Precursor Approaches. *Angew. Chem., Int. Ed.* **2013**, *52*, 11034−11039.
(31) Yu, K.; Liu, X.; Chen, Q. Y.; Yang, H.; Yang, M.; Wang, X.; Wang, X.; Cao, H.; Whitfield, D. M.; Hu, C.; Tao, Y. Mechanistic Study of the Role of Primary Amines in Precursor Conversions to Semiconductor Nanocrystals at Low Temperature. *Angew. Chem., Int. Ed.* **2014**, *53*, 6898−6904.
(32) Yu, K.; Liu, X.; Qi, T.; Yang, H.; Whitfield, D. M.; Chen, Q. Y.; Huisman, E. J. C.; Hu, C. General Low-Temperature Reaction Pathway from Precursors to Monomers before Nucleation of Compound Semiconductor Nanocrystals. *Nat. Commun.* **2016**, *7*, 12223.

DOI: 10.1021/acs.jpclett.8b01520
J. Phys. Chem. Lett. 2018, 9, 3660−3666